

## Article

# Numerical Analysis of an Innovative Double-Strap Joint for the Splicing of Near-Surface Mounted Fiber-Reinforced Polymer Bars for Reinforced Concrete Beam Strengthening

Slobodan Ranković, Andrija Zorić \* , Todor Vacev and Žarko Petrović

Faculty of Civil Engineering and Architecture, University of Niš, Aleksandra Medvedeva 14, 18000 Niš, Serbia

\* Correspondence: andrija.zoric@gaf.ni.ac.rs

**Abstract:** The issue of the cut-off splicing of an additional fiber-reinforced polymer (FRP) bar in the near-surface mounted (NSM) technique for reinforced concrete (RC) beam strengthening exposed dominantly to bending is insufficiently investigated. A possible solution of this issue is a new proposed technique: a double-strap joint. It implies the widening of the groove at the cut-off location and the symmetrical installing of additional supplements of FRP reinforcement. In this research, beam strength has been determined for the following cases: additional NSM FRP reinforcement without a cut-off, with a cut-off, and without overlapping, and with different lengths of splice overlapping. A nonlinear analysis based on the finite element method (FEM) has been applied. The length of the cut-off splice of the additional FRP reinforcement with glass fibers (GFRP) was 20Ø, 40Ø, and 60Ø. The validation of the numerical model and a comparison of the results were conducted by using the authors' experiments. It has been shown that, in the case of a cut-off of NSM GFRP bars, a significant loss in strengthening efficiency occurs, and that, with an increase in the overlapping length, this loss decreases. An overlapping length of 60Ø provides full strengthening. An efficiency assessment was carried out via the use of a parametric study, varying the FRP bar material type and its diameter for a constant splicing length.

**Keywords:** FEM analysis; double-strap joint; NSM FRP strengthening; FRP reinforcement cut-off; RC beams



**Citation:** Ranković, S.; Zorić, A.; Vacev, T.; Petrović, Ž. Numerical Analysis of an Innovative Double-Strap Joint for the Splicing of Near-Surface Mounted Fiber-Reinforced Polymer Bars for Reinforced Concrete Beam Strengthening. *Appl. Sci.* **2023**, *13*, 12387. <https://doi.org/10.3390/app132212387>

Received: 30 September 2023  
Revised: 7 November 2023  
Accepted: 14 November 2023  
Published: 16 November 2023



**Copyright:** © 2023 by the authors. Licensee MDPI, Basel, Switzerland. This article is an open access article distributed under the terms and conditions of the Creative Commons Attribution (CC BY) license (<https://creativecommons.org/licenses/by/4.0/>).

## 1. Introduction

Fiber-reinforced polymer (FRP) materials have been used for many years for repairing and strengthening reinforced concrete (RC) and prestressed structural elements exposed to bending and/or shear. Many design codes, such as those in [1–3], treat problems related to the application of FRPs in RC structures and give basic guidelines for their use. This being the case, two basic methods are applied: the externally bonded (EB-FRP) method and the near-surface mounting (NSM FRP) method. The EB-FRP method appeared earlier and has wider applications because of its practical values [4]. On the other hand, the NSM FRP method has significant advantages, which have been shown in many studies [5–9]. The basic advantage of the NSM FRP technique of strengthening compared to that of EB-FRP is based on its better adhesiveness, which mostly affects the ultimate strengths of strengthened structures [10–12]. One of the recent investigations regarding the EB and NSM FRP techniques, which is mainly concerned with the bond effect, is international research [13] in which 11 laboratories and seven manufacturers took part. In the mentioned paper, experimental results have been discussed and compared in order to examine the following: (1) the bonding of NSM strips and bars, (2) the influence of alternative single-bond or double-bond shear pulling setups that were adopted by the participating laboratories, and (3) the influence of different concrete mixture qualities coming from different countries on concrete strength. It has been concluded that the greatest influences on the bond strength are the axial stiffness and surface treatments of

FRP NSM systems. Nevertheless, there are other factors that influence the bond effect, such as the groove dimensions, epoxy type, FRP type, and concrete quality [14–16].

In addition to the above, the application of the NSM FRP technique for strengthening RC structures significantly improves the protection of FRP strengthening with regard to high temperatures and vandalism [17,18]. In addition to the NSM FRP strengthening technique, the time-dependent variation in the corrosion resistance of basalt fiber-reinforced polymer (BFRP) bars reinforced geopolymer concrete in a seawater environment has also been investigated. It has been concluded that geopolymer concrete possesses better corrosion resistance compared to Portland cement concrete, while the reduction in BFRP bars' ultimate strength in seawater is directly proportional to the bar diameter [19].

The problem of the splicing of the cut-off of FRP bars is present in cases of long structural elements and in cases of bar diameters greater than  $\varnothing 10$  mm, considering the limited transport length (10–12 m) and the impossibility of winding into coils [20]. To the best knowledge of the authors, the problem of the splicing of the cut-off of FRP reinforcement has not been treated sufficiently in the literature when it comes to the NSM method. It has been limited primarily to the investigation of anchoring length; that is, the bond effect [21,22]. This, among other things, is also concerned with numerical testing [23–26]. Recommendations for required anchoring lengths in cases of the classical way of cut-off splicing via longitudinal overlapping (as for steel reinforcement) relate to manufacturer's data for specific materials, shapes, and surface treatments of the additional FRP reinforcement [20], and relate to limited classic lap splice research recommendations [27–29].

The aim of this research was the prediction of the behavior of beams strengthened via NSM FRP reinforcement with the splicing of an NSM FRP reinforcement cut-off in the bending zone. For the splicing of an NSM FRP reinforcement cut-off, the authors proposed a new method, called double-strap joint NSM FRP. This method implies the widening of the groove in the FRP bar cut-off zone and setting two FRP supplement bars symmetrically. The connection of the supplement and main FRP bars, as well as with concrete, is provided using epoxy. The theoretical foundation for the splicing technique is represented by the force transfer between concrete and epoxy matrices, and, furthermore, between epoxy and FRP bars, which is known as the bond effect. The bond mechanism is achieved primarily through three components: adhesion, friction, and the mechanical interaction of materials. The bond failure may occur due to the epoxy failure or concrete failure in the interaction zone. The stress–strain state describing the bond effect is three-dimensional and complex. Therefore, the theory of bonds, as well as the different analytical and numerical models for bond capacity, were the subjects of the research in the last few decades [29–35].

Using a non-linear numerical analysis based on the finite element method (FEM), cases of cut-off splicing via additional bar-shaped FRP reinforcement have been analyzed; the length of the additional reinforcement took values of  $20\varnothing$ ,  $40\varnothing$ , and  $60\varnothing$ . The validation of the numerical model and the comparison of the results have been conducted using the experiments of the authors. For such a validated numerical model, the influence of the diameter and type of NSM FRP bars on the strength and stiffness of the beams has been investigated. The overlapping length of the splicing for achieving the full strength of the beams has also been determined. The behavior of the beams strengthened by glass FRP (GFRP) and carbon FRP (CFRP) bars with an equal diameter ( $\varnothing 10$ ) in cases of cut-off splicing with an equal supplement length ( $60\varnothing$ ) has been compared. Finally, the economic feasibility of the proposed method has been briefly presented.

The proposed double-strap joint NSM FRP splicing method's technological preparation is as simple as needed for practical engineering applications. On the other hand, this technique provides symmetrical load transfer in the zone of an FRP bar cut-off, which is an advantage over the conventional longitudinal splicing method. This paper is intended to fully confirm the structural advantages of this method and to propose recommendations for its application in engineering practice, as well as to support currently limited research on the FRP splicing problem.

## 2. Materials and Methods

### 2.1. Experimental Research

#### 2.1.1. Experimental Specimens

The complete procedure of the newly proposed method of cut-off splicing of additional bar-shaped GFRP reinforcement for beam strengthening, called double-strap joint NSM FRP, has been given in the authors' previous paper [16]. The beam specimens have been tested under a four-point load disposition (Figure 1a), where the following beams have been tested: (1) B-CON beam, with steel reinforcement only and without FRP strengthening (Figure 1b); (2) B-G1 beam, strengthened within the concrete cover via NSM GFRP without a cut-off and a diameter of  $\varnothing 10$  mm (Figure 1c); (3) B-G2 beam, with a cut-off of the strengthening bar in the midspan of the beam ( $L/2$ ) and without bypassing (Figure 1c); (4) B-G3 beam, with a cut-off of the strengthening bar in  $L/2$  and with bypassing on both sides,  $2 \times \varnothing 10$ , and 20 cm long (Figure 1d); and (5) B-G4 beam, with a cut-off of the strengthening bar in  $L/2$  and with bypassing on both sides,  $2 \times \varnothing 10$ , and 40 cm long (Figure 1d). The specimens were made of concrete with a compression strength of 31.6 MPa and with steel reinforcement with a yield strength of 400 MPa. The groove for the strengthening was cut in the specimens and GFRP bars were placed, while a MapeWrap11 epoxy was used (Figure 2). Considering that the maximal bending moment is in the middle third of the beam span, and that it decreases towards the beam supports, the development length of the straight FRP bar in the ending third of the span is sufficient for the anchoring and force transfer from the FRP bar to the epoxy and then on concrete. Consequently, the bond mechanism [29,33] provides composite action of the concrete, epoxy, and FRP bar.

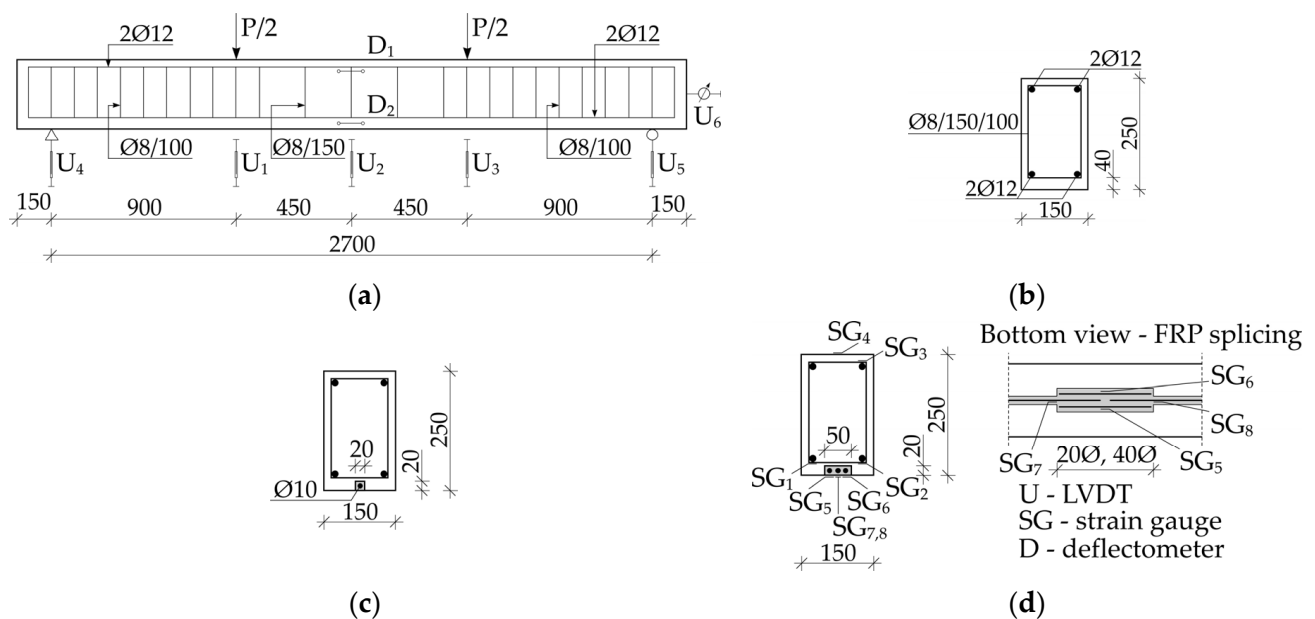


**Figure 1.** Experimental specimens: (a) beam disposition; (b) cross-section of an unstrengthened beam (model B-CON); (c) cross-section of a strengthened beam without a cut-off (model B-G1) and a strengthened beam with a cut-off and without bypassing (model B-G2); and (d) cross-section of a strengthened beam with a cut-off and with different lengths of bypassing (models B-G3 and B-G4).

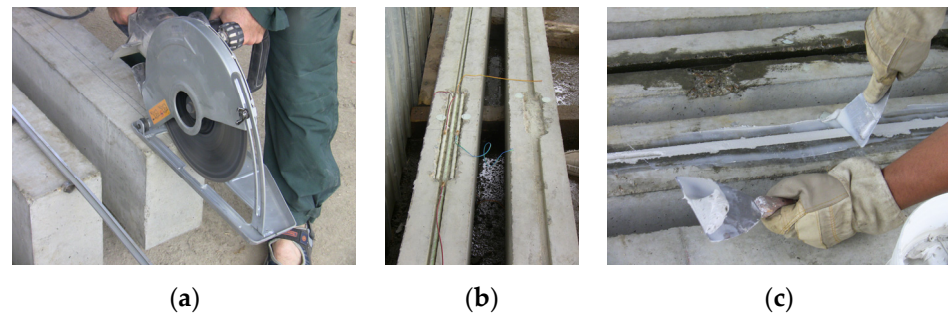


**Figure 2.** Preparation of the test specimens: (a) cutting of the groove for GFRP strengthening; (b) FRP installation and detail of the double-strap joint; and (c) epoxy installation.

### 2.1.2. Experimental Testing

The samples have been tested via the continual application of load by a hydraulic press, where the test was in the “displacement control mode” with a constant growth rate of deflection of 0.02 mm/s. Deflection was measured via linear variable displacement transducers (LVDTs), while the strains in concrete, as well as in steel and GFRP reinforcement, have been recorded using LVDTs with a base of 100 mm and strain gauges with a base of 6 mm. A data acquisition system with an automatic data-reading period of 1 s has been used for measure sampling. The measuring setup scheme has been presented in Figure 1a,d, and the specimen during the testing has been presented in Figure 3.

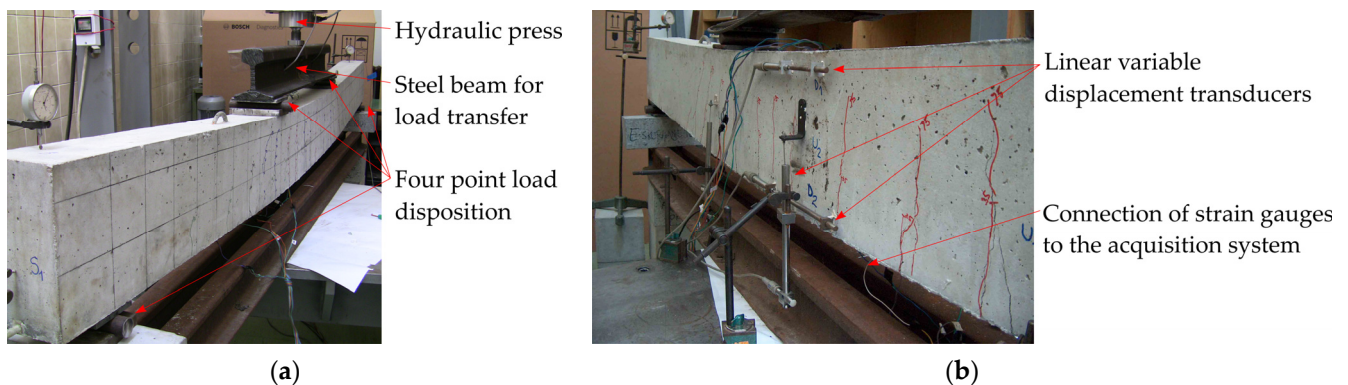


**Figure 3.** Experimental test: (a) front view of test specimen; (b) back view of test specimen with instruments.

The results of the experimental tests of the strengthening effects, with and without a cut-off of additional NSM GFRP reinforcement, and a comparison with a control (unstrengthened) beam have been obtained. The analysis of results encompassed presenting the strength and stiffness of the tested specimens, as well as the strains in the tensioned basic (steel) and additional (GFRP) reinforcement, as well as those in the concrete. Additionally, a presentation of the failure mechanism of the tested specimens for different strengthening configurations regarding the occurrence and propagation of cracks has been provided. It was concluded that the absence of cut-off splicing provides beam failure due to a dominant crack at the cut-off location, while when introducing the double-strap joint splicing the failure occurs at the endings of the supplement grooves via concrete peeling-off. For details of the experimental program and experimental results, the reader is referred to reference [16].

## 2.2. Finite Element Modeling

### 2.2.1. Model Description

In this research, a numerical model for analyzing the RC beams strengthened via the NSM method with FRP bars and the innovative double-strap joint has been proposed



through the use of the FEM and Abaqus/Standard 6.13 software. The model validation has been conducted by comparing the load–deflection diagrams for all of the experimentally tested beam cases, as well as load–strain diagrams for GFRP bars in model B-G4. The proposed numerical models have also been used for a parametric analysis of the strengthened RC beams.

The geometry of the FE models of the RC beams has been created according to the geometry of the test beams (Figure 1) [16]. The geometry of beam B-G3 has been presented in Figure 4a, and the geometry of the reinforcement and GFRP bars has been presented in Figure 4b. The geometry of all other beams is analogous, except for some small changes in the epoxy and GFRP geometry due to the (non)existence and length of the double-strap joint.

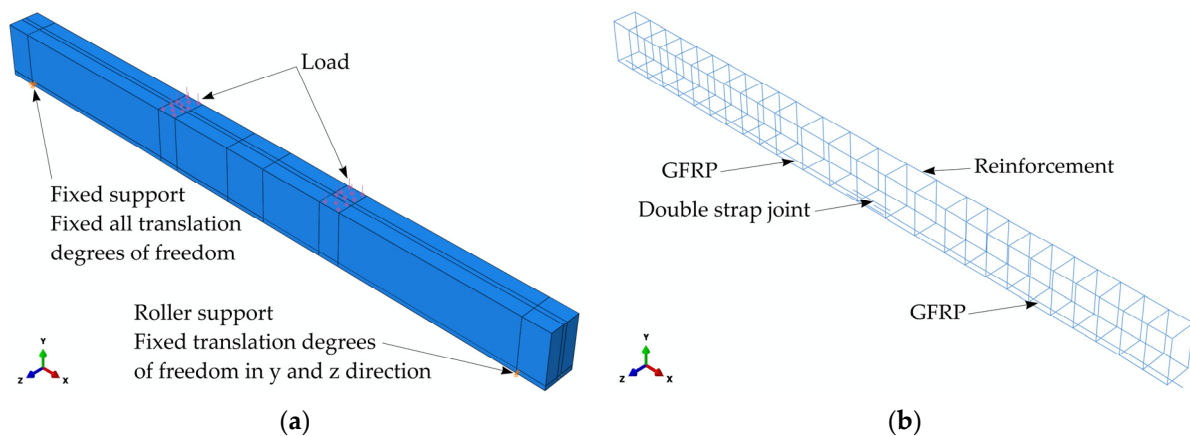


**Figure 4.** FE model B-G3: (a) beam geometry and boundary conditions; (b) geometry of reinforcement and GFRP bars.

In the experimental setup, one end of the RC beams had pinned support, and the other end had roller support. These supports were not modeled in detail, but appropriate boundary conditions have been defined. Namely, in the support axes, at a distance of 150 mm from the beam ends, the displacements of the nodes at the bottom side of the beam have been restrained. For the pinned support, all three translations have been restrained, and for the roller support, only vertical and lateral translations have been restrained (Figure 4a). In the experimental tests, load has been applied via steel plates set at thirds of the span. In the numerical models, this was simplified, such that steel plates were omitted, but the load has been applied as surface load across the top surface of the concrete beams (Figure 4a).

The mechanical properties of concrete (compression strength and modulus of elasticity), as well as the tensile strength and modulus of elasticity of GFRP and steel reinforcement bars have been experimentally determined [16], and they are presented in the following sections of the article.

### 2.2.2. Material Model of Concrete

In this research, the concrete material has been modeled via the use of a concrete damage plasticity (CDP) material model. The stress–strain diagram ( $\sigma_c - \epsilon_c$ ) of concrete under compression (Figure 5a) was defined based on recommendations [36], such as the following equation:

$$\sigma_c = \frac{k\eta - \eta^2}{1 + (k - 2)\eta} f_c; \quad \eta = \frac{\epsilon_c}{\epsilon_{c1}}; \quad k = 1.05E_c \frac{\epsilon_{c1}}{f_c}, \quad (1)$$

where the following is the case:

$\epsilon_{c1} = 0.00205$ , which is the strain at the maximal stress.

$\varepsilon_{cu1} = 0.00350$ , which is the ultimate strain.

$f_c = 31.60$  MPa, which is the compressive strength.

$E_c = 32.80$  GPa, which is the modulus of elasticity.

The elastic behavior of the analyzed concrete under compression was  $0.4f_c = 12.64$  MPa (with a correspondent strain of 0.000385).

The characteristics of the concrete under tension ( $\sigma_t - \varepsilon_t$  diagram) have been defined via the use of the relation given in [37]:

$$\sigma_t = f_t \left( \frac{\varepsilon_{cr}}{\varepsilon_t} \right)^{0.40}, \quad (2)$$

where the following is the case:

$f_t$  is the concrete tensile strength.

$\varepsilon_{cr}$  is the strain at the concrete tensile strength.

The tensile strength of concrete ( $f_t$ ) has been defined according to the relationship proposed in [38], and by compressive strength ( $f_c$ ):

$$f_t = 0.34\sqrt{f_c} = 0.34\sqrt{31.60} = 1.911 \text{ MPa}. \quad (3)$$

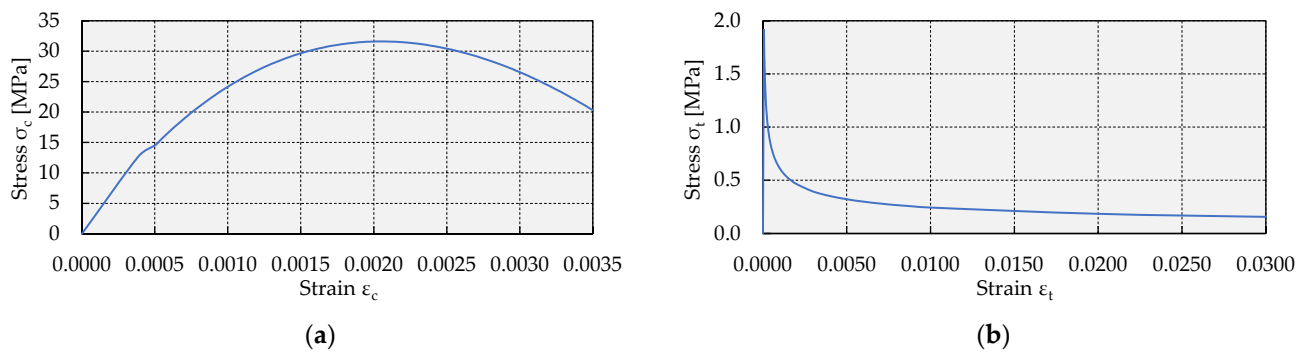


**Figure 5.** Stress–strain diagram for concrete: (a) compression; (b) tension.

The strain that corresponds to the tensile strength was  $\varepsilon_{cr} = 0.00005826$ . This value defines the boundary of the elastic behavior of the analyzed concrete under tension. A stress–strain diagram of the concrete under tension is presented in Figure 5b.

The plastic behavior of concrete is described as the damage of concrete due to both compression and tension in the adopted CDP model. This model has been selected as adequate for modeling quasi-brittle materials [39–41]. Several input parameters need to be defined for the CDP material model, and these values are adopted according to the recommendations [39–41] and presented in Table 1.

**Table 1.** Input parameters for the CDP material model.

Parameter	Value
Dilation angle, $\psi$	30°
Flow potential eccentricity, $e$	0.1
Ratio of the biaxial compressive and uniaxial compressive yield stress, $\sigma_{b0}/\sigma_{c0}$	1.16
Ratio of the second stress invariant on the tensile meridian to that on the compressive meridian at initial yield, $K$	0.666
Viscosity parameter, $\mu$	0.0001

The CDP model enables the reducing of the initial modulus of elasticity that arises owing to concrete damage. This is realized by means of damage parameters for compression,  $d_c$ , and for tension,  $d_t$  [39,42], and they are determined by the following relations:

$$d_c = 1 - \frac{\sigma_c}{f_c}; \quad d_t = 1 - \frac{\sigma_t}{f_t}. \quad (4)$$

Damage parameters have been defined with respect to inelastic strains,  $\varepsilon_c^{in}$ , and with respect to cracking strains,  $\varepsilon_t^{cr}$ , for compression and tension, respectively (Figure 6). Based on these data, the plastic strain in compression and tension have been calculated by software [39].

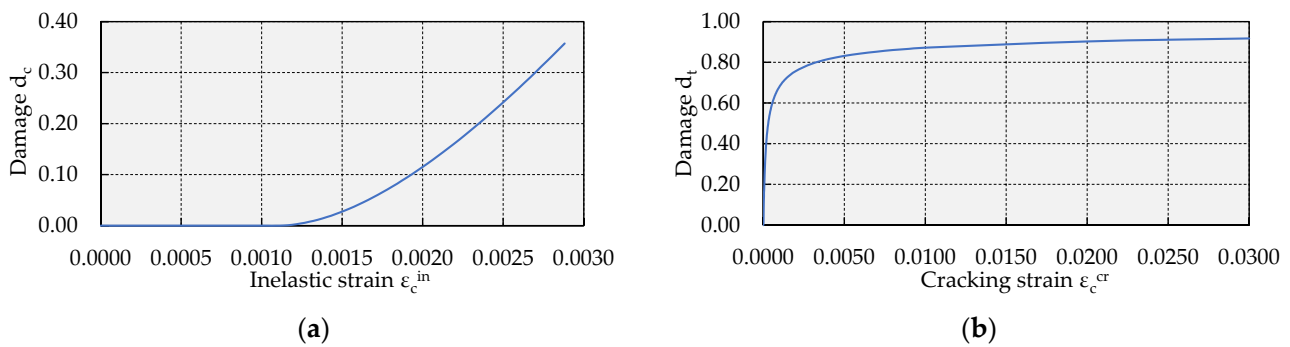


**Figure 6.** Damage parameters in the CDP model of concrete: (a) compression; (b) tension.

### 2.2.3. Material Model of Epoxy

The material characteristics of the epoxy have been modelled with the same material model used for concrete, i.e., the CDP material material model. All of the details provided in the previous Section 2.2.2, stand for the modeling of the material characteristics of the epoxy, with the remark that the modulus of elasticity is  $E_e = 4000$  MPa, the compressive strength,  $f_{ce}$ , is 70 MPa, and the tensile strength,  $f_{te}$ , is 19.10 MPa. All of these parameters have been adopted according to the manufacturer's data [20]. The stress–strain diagrams of the epoxy at compression and tension are presented in Figure 7, and the dependencies of the damage parameters on strains of the epoxy are shown in Figure 8.

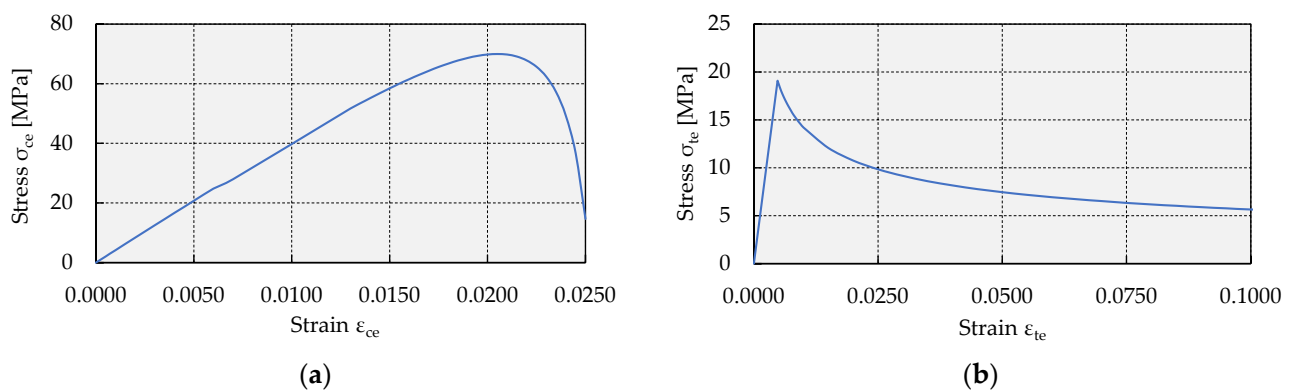


**Figure 7.** Stress–strain diagram for epoxy: (a) compression; (b) tension.

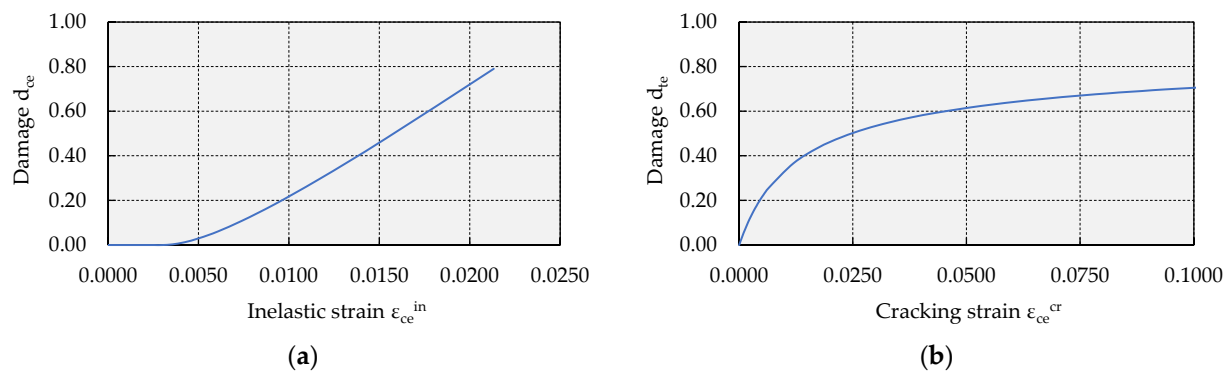


**Figure 8.** Damage parameters in the CDP model of epoxy: (a) compression; (b) tension.

#### 2.2.4. Material Model of Steel Reinforcement and GFRP Bars

For steel reinforcement, a bilinear kinematic hardening model was adopted (Figure 9a). The modulus of elasticity of reinforcement was  $E = 205$  GPa, the yield stress was  $f_y = 400$  MPa, and the tangent modulus was  $E_t = 11,828$  MPa, according to the mechanical properties of reinforcement used for the experimental specimens. The GFRP bars have been modeled as a linear elastic material with a modulus of elasticity,  $E$ , of 47 GPa, and an ultimate tensile strength,  $f_u$ , of 760 MPa (Figure 9b).

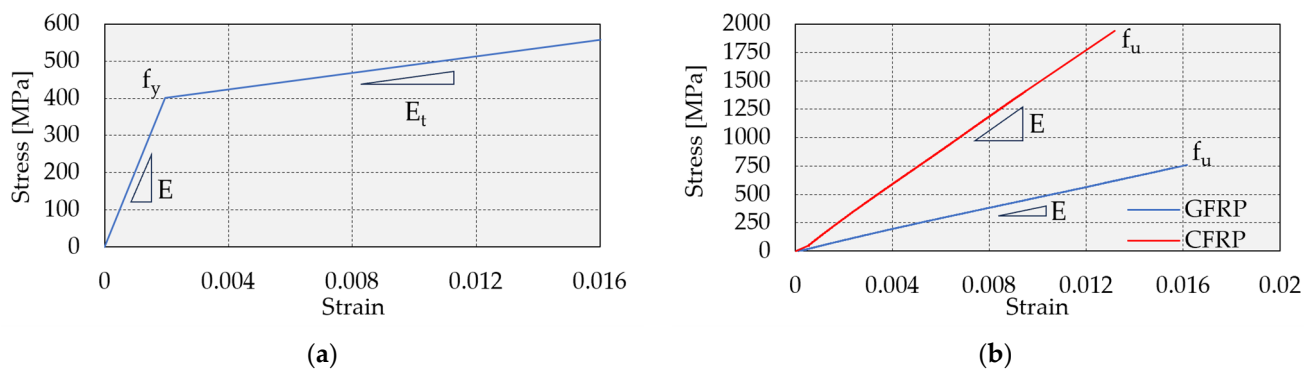


**Figure 9.** Stress–strain diagrams: (a) steel reinforcement (bilinear kinematic material model); (b) GFRP and CFRP reinforcement (linear elastic material model).

#### 2.2.5. Finite Element Mesh

The RC beam and epoxy were meshed with solid hexahedral FE with three translational degrees of freedom per node (denoted in the software as C3D8R) [39]. The “shear locking” phenomenon was prevented via reduced integration for stiffness matrix determination [39,43]. The steel reinforcement and GFRP bars have been meshed with truss FE with 2 nodes, having axial stiffness only (denoted in the software as T3D2) [39]. An appropriate cross-section area has been defined according to the diameter of longitudinal reinforcement, stirrups, and GFRP bars. A mesh convergence analysis has been conducted for model B-CON in order to check mesh sensitivity and to determine the optimal FE mesh size. In this analysis, five FE sizes have been varied, namely 12.5, 20, 25, 30, and 50 mm. For a comparative analysis, vertical displacement in the beam midspan at a load of 2500 daN has been selected. It has been concluded (Figure 10) that the mesh with an FE size of 50 mm was too coarse, and the results have become stable for an FE size lower than or equal to 30 mm. Consequently, for further research, an FE size of 25 mm has been adopted as optimal from the perspective of required computer resources and the accuracy of results. In cases of strengthened beams, the FE size for epoxy modeling was 10 mm, because of its small dimensions compared to the dimensions of the RC beam cross-section and expected stress concentration in the epoxy. The FE mesh of model B-G3 is shown in Figure 11, as a representation.



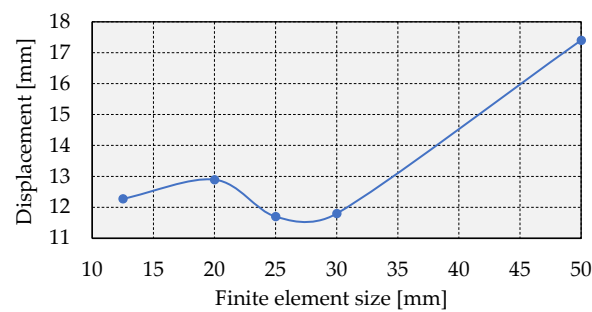


**Figure 10.** Mesh convergence analysis for model B-CON.

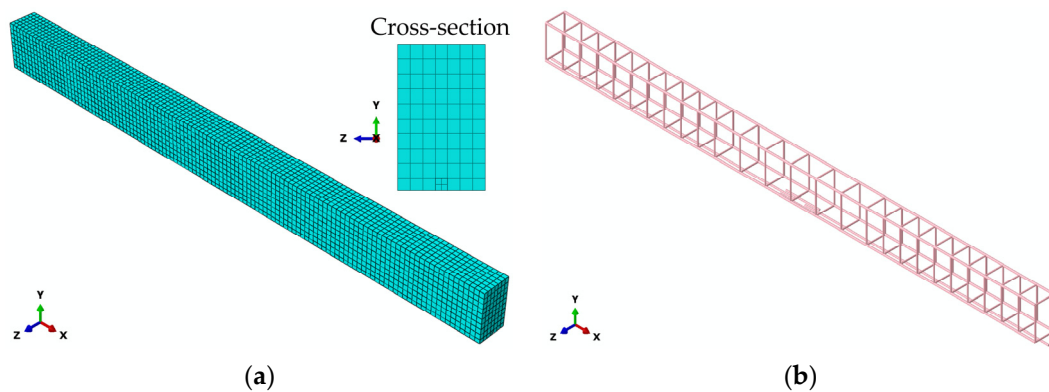


**Figure 11.** FE mesh of model B-G3: (a) beam; (b) steel and GFRP bars.

#### 2.2.6. Modeling of Interaction between Different Materials

The modeling of the interaction between the epoxy and concrete has been carried out with cohesive contact elements, as recommended in [28]; the maximal normal contact stress has been set to 70 MPa and the maximal contact shear stress to 3 MPa, according to the manufacturer's data [20]. Damage evolution has been described via fracture energy of 15 MPa, based on the available and proven models [28,44]. Interaction surfaces of epoxy and concrete are presented in Figure 12a, again for model B-G3. The contact between concrete and steel reinforcement, as well as between the epoxy and the GFRP bars, has been ideally modeled without slip, using the built-in embedded region function of the software (Figure 12b).

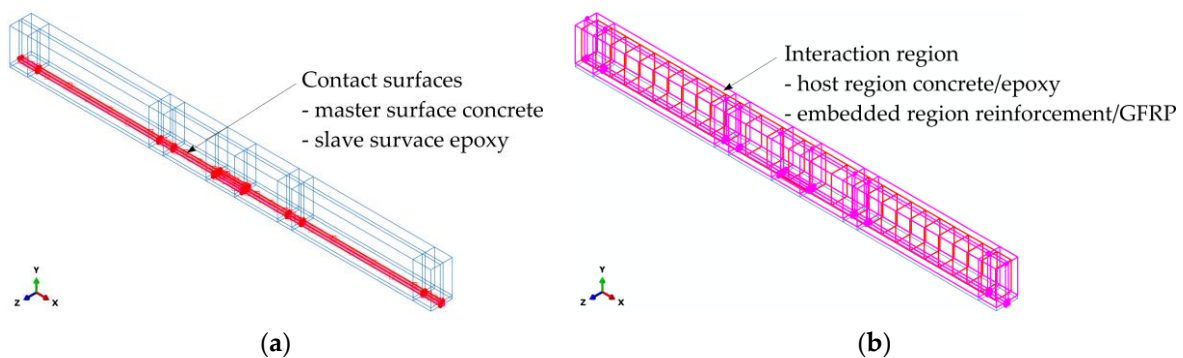


**Figure 12.** Modeling of interaction between different materials: (a) cohesive contact surfaces of concrete and epoxy; (b) bond connection between concrete/epoxy and reinforcement/GFRP.

### 3. Results and Discussion

#### 3.1. Model Validation

The validation of the numerical model has been conducted by comparing the force–deflection diagrams obtained experimentally [16] and numerically for all of the analyzed models (Figure 13a–e). Based on a comparative analysis of the numerical and experimental load–deflection ratios, one may notice very good agreement of the results up to failure, which confirmed the model validation. Full agreement of the results has been achieved in the first and second load–deflection branches for all of the analyzed models, i.e., in the elastic regime and after the crack opening up to the steel reinforcement yield. A slight disagreement of the results is noticeable in the third branch of the load–deflection diagrams. Namely, after the yield of the steel reinforcement, a sudden loss in beam stiffness occurs. Due to the highly nonlinear problem, at this stage some discrepancy in the numerical and experimental results occurs. Nonlinear phenomena in this problem are caused by concrete cracking, steel reinforcement yielding, concrete crushing in the compression zone, the bonding effect between the concrete and the epoxy, and the heterogeneity of the concrete in the experimental beams. Considering all of the abovementioned conditions, one may conclude that the obtained numerical results are in good agreement with the experimental ones. Certain deviations have been noticed for the beams B-G2 and B-G4. Model B-G2 is with the cut-off of the strengthening FRP bar in the midspan, but without bypassing (splicing). Therefore, after the steel reinforcement yield, an abrupt development of a crack in the midspan occurs, leading to the loss of the effectiveness of the additional FRP bar and causing the beam behavior to be similar to that of the control beam without FRP strengthening. This highly nonlinear effect influenced the slight disagreement in the numerical and experimental results (Figure 13c). On the other hand, model B-G4 showed somewhat higher stiffness (Figure 13e) because of the longer groove filled with epoxy, which possesses better mechanical characteristics than those of concrete. After the moment of the steel reinforcement yield and sudden crack propagation, the numerical results are stabilized, indicating a convergence towards the experimental results. Considering everything mentioned, the numerical models can be treated as reliable in the sense of the load–deflection ratios of the analyzed models.

The failure mechanism represented by crack propagation, as well as the shear stress propagation (bond stress) at the contact of the epoxy and the concrete, has also been analyzed. Exceeding this stress proved to be the main cause of failure. A comparative analysis between the numerical and the experimental test has been conducted, considering both parameters (the cracks and the bond effect). It has to be mentioned that the crack development in the CDP model has been defined via the damage parameter in tension. Other research recommends that a crack opens at strains several dozen times greater than the strain at tension strength [45,46]. In this research, the value of the damage parameter,  $d_t$ , of 0.80, which corresponds to a strain 50 times greater than the strain at tension strength, has been adopted as the crack opening.

Representative models for the analysis of the cracks and bond stresses were B-G1, without the cut-off of GFRP reinforcement, and B-G4, with cut-off bypassing realized via supplemental GFRP bars of 40Ø (40 cm) in length. One may conclude that cracks open uniformly at the strengthened beam without GFRP cut-off, and that cracks do not intersect the epoxy because it has a higher tensile strength (Figure 14). On the concrete–epoxy interface, a maximal contact shear stress of 3 MPa has been reached. As a consequence, slippage of the epoxy occurs, which leads to the relocation of the critical zone and to the redistribution of the shear stresses. This is more prominent in the region starting from the load application zone towards the supports (Figure 15). All of these results are in good accordance with the experimental ones, presented in [16]. The cracks are uniformly distributed in the case of model B-G4 (Figure 16), which indicates that the bypassing of the cut-off gives effects, and this is in concordance with the experimental results. Analogously to the experimental results [16], the numerical analysis confirmed the occurrence of the exceeding of the shear stress (bond stress) on the epoxy–concrete joint, which leads to the

concrete peeling-off. This occurs because of the increased stiffness of the cross-section at the beginning of the groove widening for inserting supplemental GFRP bars (Figure 17). On the other hand, the failure of model B-G2 (with a cut-off of the GFRP, but without bypassing) was caused by a dominant crack that extends from the bottom tension zone all the way up to the compression zone in the midspan section (Figure 18). This result is similar to the experimentally obtained one, confirming that GFRP reinforcement with a cut-off but without splicing has a marginal influence on beam strengthening.

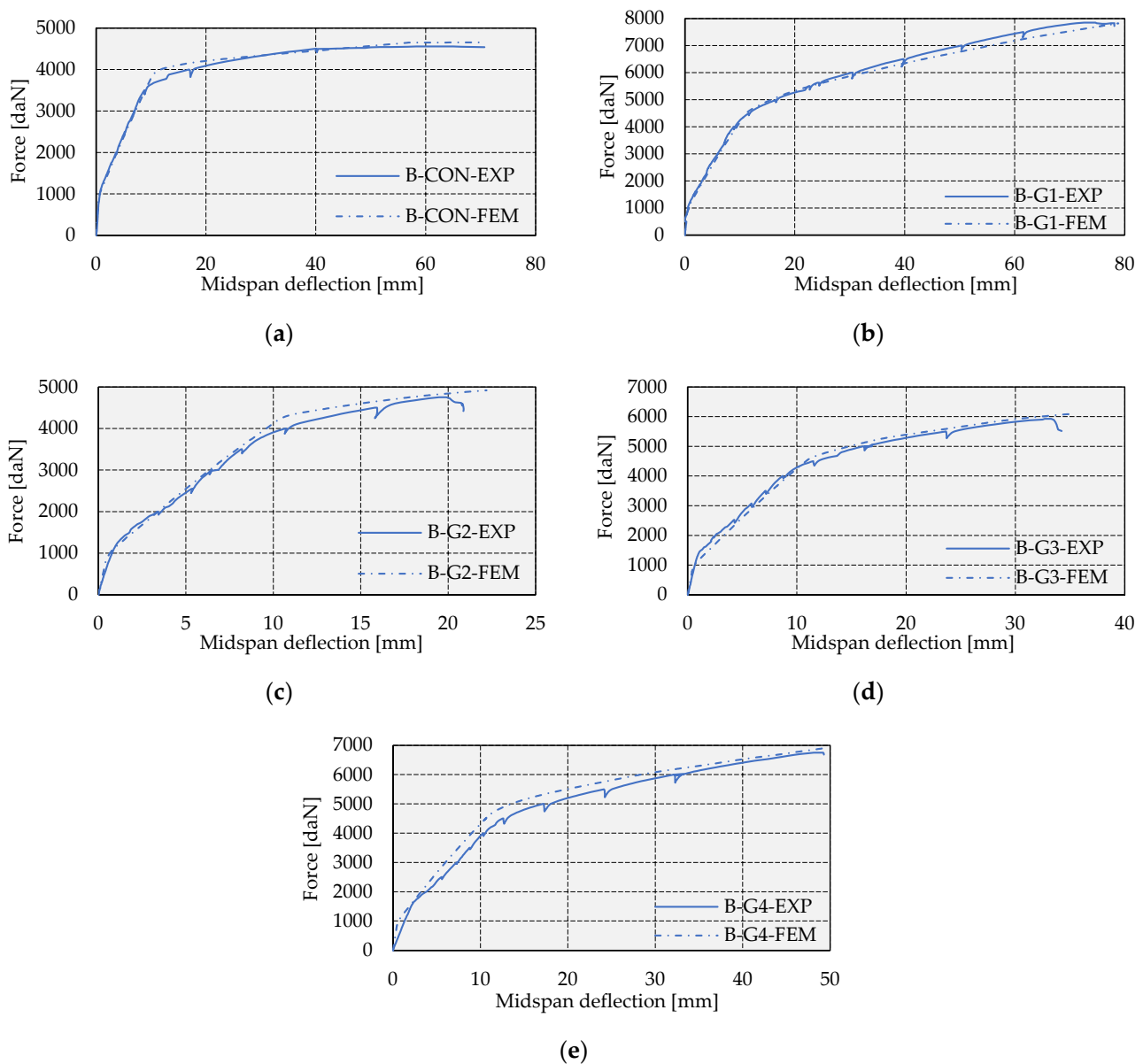


**Figure 13.** Comparative analysis of the force–deflection diagrams: (a) B-CON; (b) B-G1; (c) B-G2; (d) B-G3; and (e) B-G4.

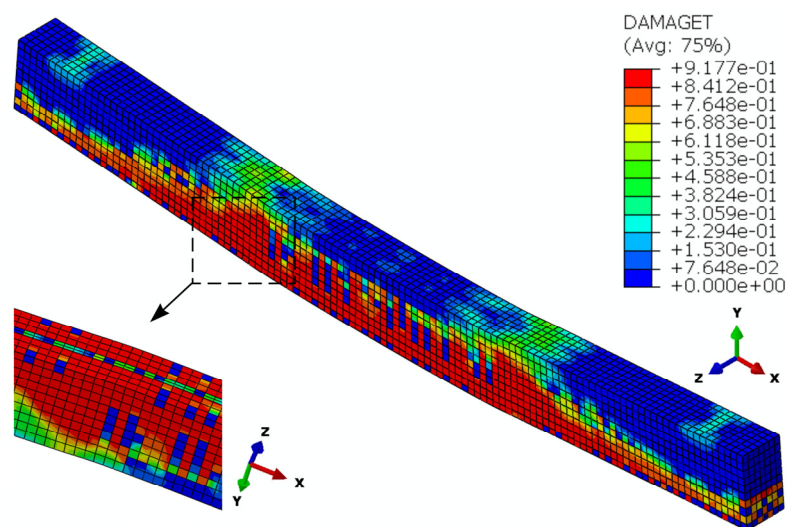


Figure 14. Damage parameter in tension for model B-G1.

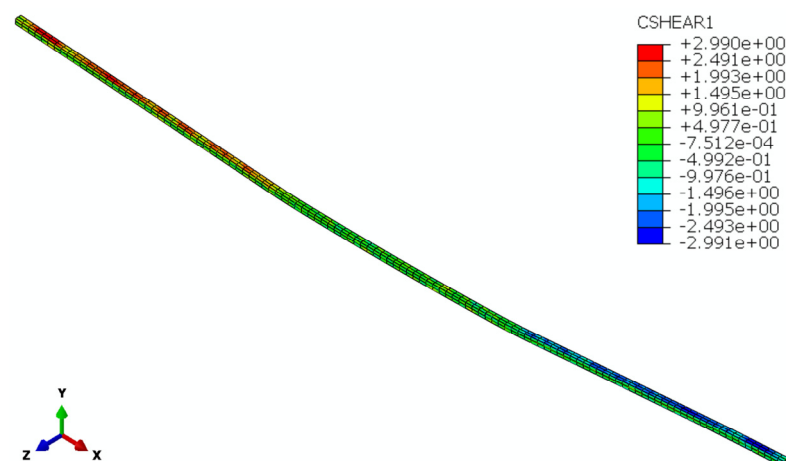


Figure 15. Shear stress (bond) at the concrete–epoxy interface for model B-G1.

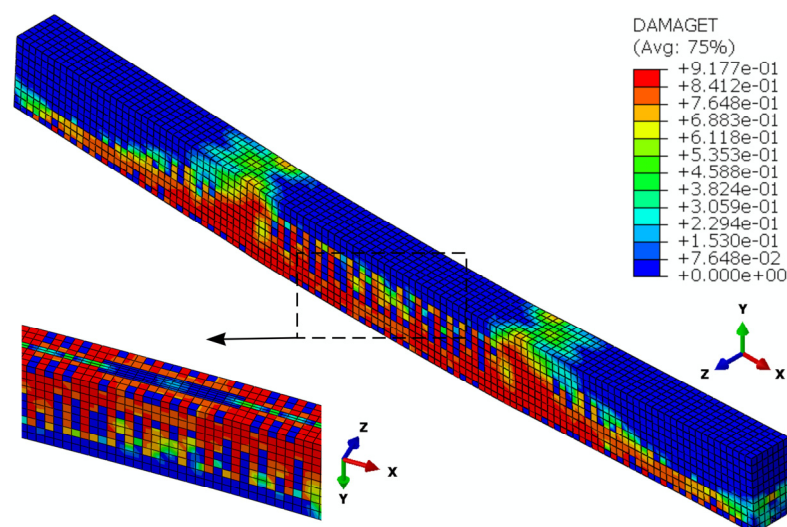
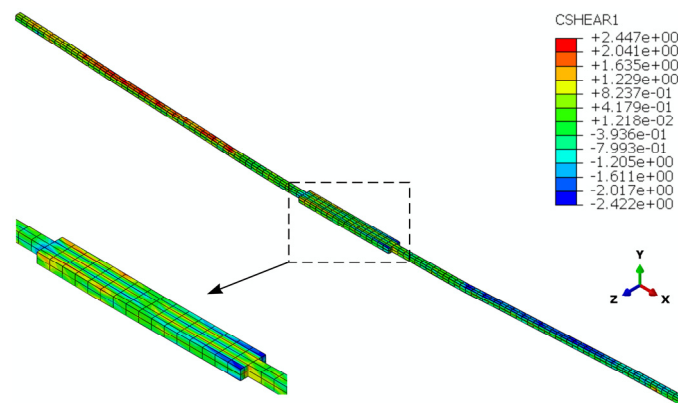
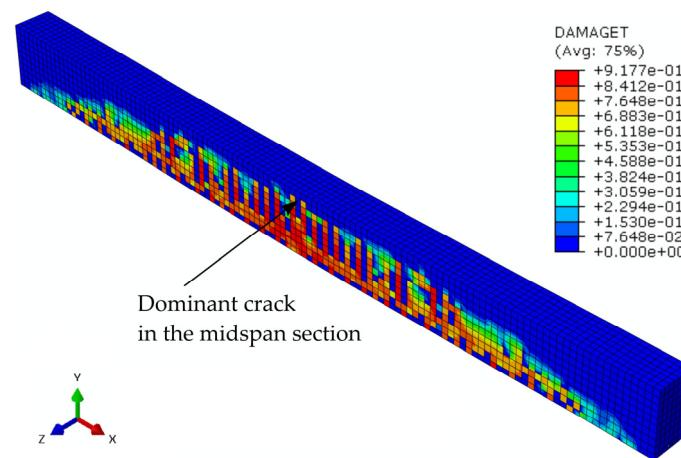


Figure 16. Damage parameter in tension for model B-G4.





**Figure 17.** Shear stress (bond) at the concrete–epoxy interface for model B-G4.



**Figure 18.** Damage parameter in tension for model B-G2.

The final step in the validation of the numerical model was a comparison of the strains in the GFRP bars with the experimentally obtained results for model B-G4 (Figure 19). It could be concluded that there was satisfactory agreement of the numerical and experimental results in the case of the main GFRP bars, and a slight discrepancy in the results in the case of the GFRP strap joint. Considering the high nonlinearity of the problem, which depends on several physical and mechanical parameters, one may consider that the agreement was satisfying, thus confirming the validity of the numerical model.

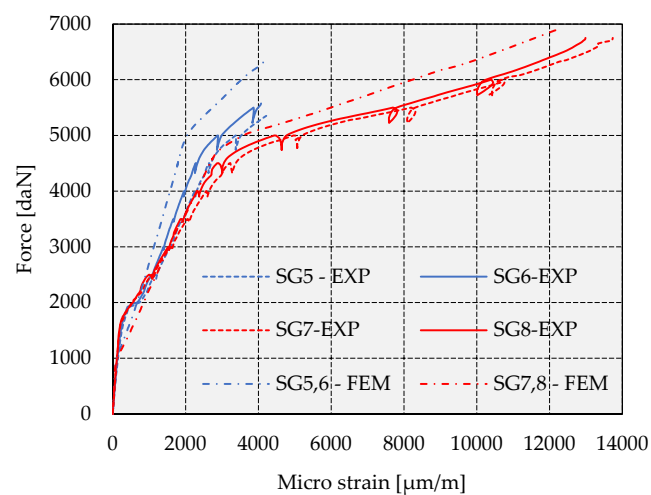


**Figure 19.** Strains in the GFRP bars and GFRP strap joint for model B-G4.

### 3.2. Numerical Analysis of the Required Splicing Length of the GFRP

Based on the experimentally obtained results and linear extrapolation [16], it has been determined that the length of the supplement of 60Ø (60 cm) provided beam strength equal to the beam without a GFRP cut-off. An NSM GFRP bar spliced in this way has the same strengthening effect as a GFRP reinforcement without a cut-off. The extrapolation method is not reliable enough; therefore, one of the main goals of this paper was to confirm this conclusion completely, based on a developed and validated numerical model. According to the postulates presented in Section 2.2., a numerical model of a beam strengthened by GFRP reinforcement with both-sided overlapping at the cut-off location with a length of 60 cm has been created. The ground for determining the efficiency of the strengthening was a comparative analysis of a load–deflection diagram. Figure 20 presents, side-by-side, the experimental and numerical load–deflection diagram for the beam without a cut-off of GFRP reinforcement (B-G1), and for the beam with splicing overlapping of 60 cm. Based on the results, one may conclude that elastic stiffness and stiffness after crack occurrence coincide completely. The stiffness of the beam after the yielding of the basic reinforcement is in good correlation with the experimental results.

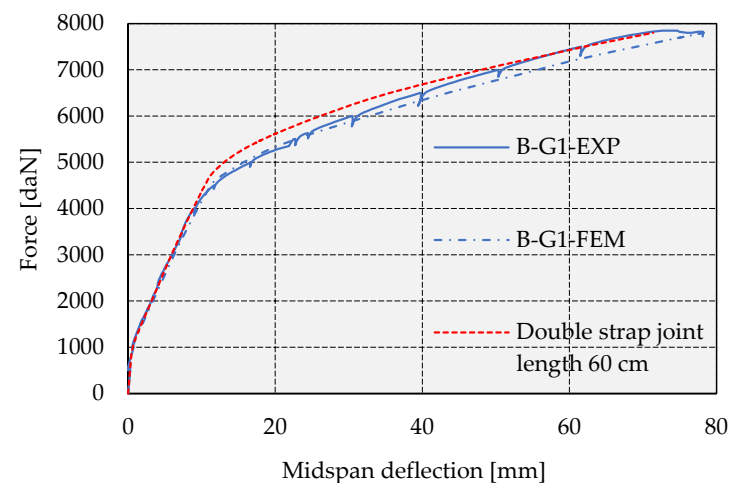


**Figure 20.** Comparative analysis of the force–deflection diagram of model B-G1 and the model with a double-strap joint length of 60 cm.

One may notice that the beam with a double-strap joint of 60 cm exhibits an approx. 5% greater force value at the occurrence of the yield of the basic reinforcement. Additionally, at the ultimate load the deflection in the midspan is about 10% lower. The reason for such results is the increase in the overlapping length, i.e., of the groove, which contains the epoxy and two inserted FRP bars, and thus exhibits higher stiffness and lower beam ductility. An increased groove length increases the adhesion at the joint between the concrete and the epoxy, and, at the same time, the epoxy also has a higher tensile strength compared to that of concrete. This is manifested after the occurrence of the yielding of the basic reinforcement (steel), which can be seen on the diagram in Figure 20.

The confirmation of the conclusion regarding the failure mechanism has been conducted through the analysis of the crack pattern, expressed as the damage parameter in tension, as well as through observing the shear (bond) stress at the concrete–epoxy interface. The results of the analyzed model with a GFRP splicing length of 60 cm (Figures 21 and 22) have been compared with the results of model B-G1 (Figures 14 and 15). The analysis results show that the crack pattern is uniform, similar to beam B-G1. The obtained shear (bond) stresses at the concrete–epoxy interface confirm that this stress has been exceeded at the beginning of the widening of the groove for cut-off bypassing, as well as in the zone starting from the load application towards the supports. This indicates that the failure mode of the concrete beam with a GFRP splicing of 60 cm is the same as in the remained splicing cases (B-G3 and B-G4). It is worth mentioning that, in the numerical models, the

tensile strength of the GFRP reinforcement is also achieved at the ultimate load, which is in concordance with the experimentally measured strains in the GFRP reinforcement of beam B-G1 [16].

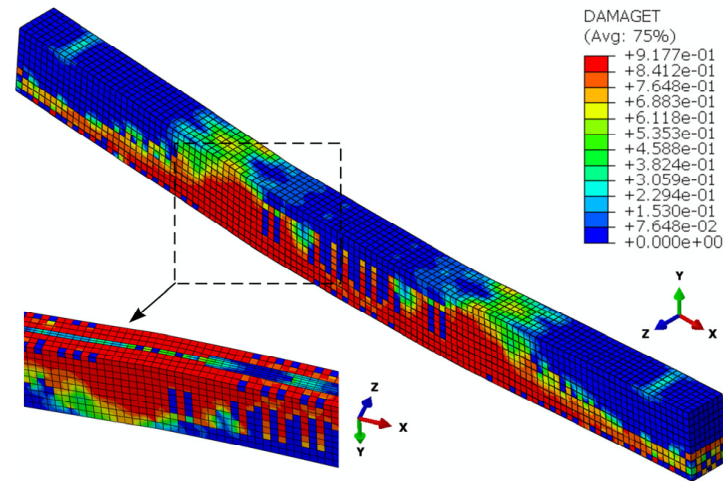


**Figure 21.** Damage parameter in tension for a model with a double-strap joint length of 60 cm.

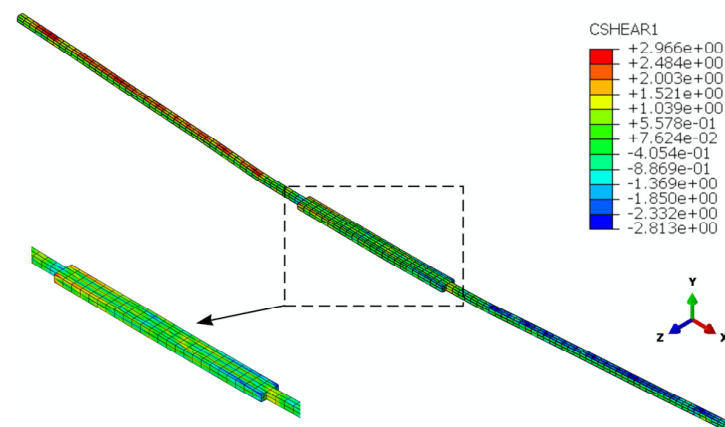


**Figure 22.** Shear stress at the concrete–epoxy interface for a model with a double-strap joint length of 60 cm.

Based on these results, one may confirm that the complete splicing of a GFRP reinforcement with a cut-off in the system double-strap joint can be achieved via the use of supplemental bars with a length of  $60\varnothing$ . Compared to the required overlapping length of  $110\varnothing$  in the classic lap splice method [28], it can be concluded that the proposed splicing method requires less overlapping length to achieve the same bearing capacity as in the case of NSM FRP strengthening without a cut-off of the additional FRP bar. It should be mentioned that some research proposes overlapping lengths of  $70\varnothing$ – $90\varnothing$  and  $40\varnothing$ – $50\varnothing$  in the classic lap splice method of CFRP bars and GFRP bars, respectively, but the research is focused on the splicing of FRP bars as reinforcement of flexural concrete members, but not on the NSM FRP strengthening technique [27].

### 3.3. Parametric Study

The validated numerical model presented in Section 2.2. has been applied for a parametric study of the influence of the diameter and type of FRP bars (glass and carbon) on the mechanical characteristics of the strengthened beams without a cut-off. Furthermore, a parametric analysis of the influence of the type of FRP bar on beam strength has been conducted for a constant length of double-strap joint splicing of  $60\varnothing$ .

Within the parametric analysis of the influence of the diameter of FRP bars without a cut-off on the characteristics of the strengthened beams, cases with diameters of Ø8, Ø10, and Ø12 have been analyzed. For all of the quoted bar diameters, an analysis with glass (GFRP) and carbon (CFRP) fibers has been conducted, taking the values of the modulus of elasticity,  $E = 148.10$  GPa, and the ultimate tensile strength,  $f_u = 1940$  MPa, for the CFRP bars (Figure 9b). Although the different FRP types, reflected in different stress–strain relationships (Figure 9b), as well as surface treatments, influence the bond strength [14,34], it is considered to be the case that the anchoring length of FRP bars in the first and third sections of the beam span is sufficient to provide composite action. Figure 23 presents force–deflection diagrams obtained numerically. One may conclude that, in cases of applications of GFRP without a cut-off, with an increase in the diameter from Ø8 to Ø10, and finally to Ø12, strength is increased by about 10%. Compared to the beams strengthened with GFRP bars, the beams strengthened with CFRP bars with the same diameter produce higher strength and stiffness of the beam, but lower beam ductility (ratio of the displacement at the ultimate load and the displacement at the yield of the primary steel reinforcement). The reason for this is the higher modulus of elasticity of the CFRP reinforcement, as well as the higher bond stress at the concrete–epoxy joint, which lead to more brittle failure compared to the case of beam strengthening with the GFRP bars. With an increase in the CFRP bar diameter, strength is increased for about 5%, which represents a slightly lower value compared to the strength increase in the case of the application of GFRP bars. It should be mentioned that, for the smallest diameter (Ø8), the application of CFRP instead of GFRP bars provides higher beam strength for approximately 20%. This effectiveness decreases with an increasing FRP bar diameter. Nevertheless, the choice between the application of the GFRP and CFRP bars for RC beam strengthening should be protracted by cost analysis as well, considering the higher price of CFRP bars.

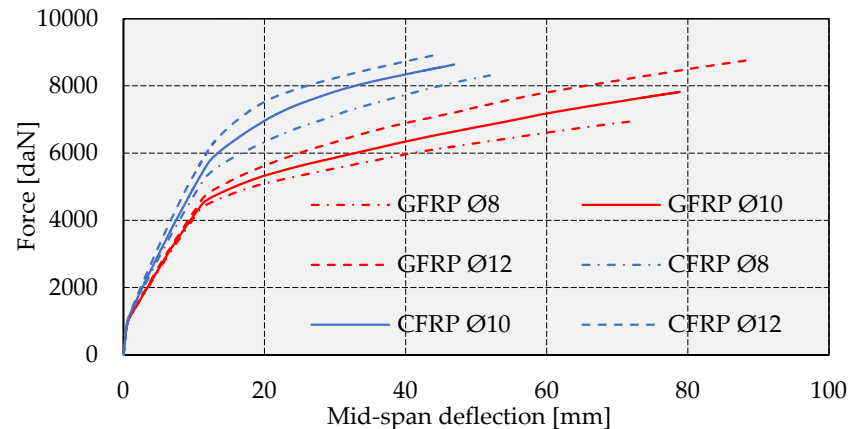


**Figure 23.** Influence of the diameter and type of FRP bar without a cut-off on the strength and stiffness of the strengthened beams.

The result of the analysis of the influence of the fiber type (GFRP, CFRP), for a constant bar diameter (Ø10) and for an overlapping length of  $60\phi$ , is that it provides strength of a strengthened beam equal to the case of a beam with an FRP bar without a cut-off (Figure 24). This result fully confirms the conclusion that an overlapping length of  $60\phi$  is required for the same strengthening effect as in the case of a beam without an FRP bar cut-off, regarding the FRP bar type.



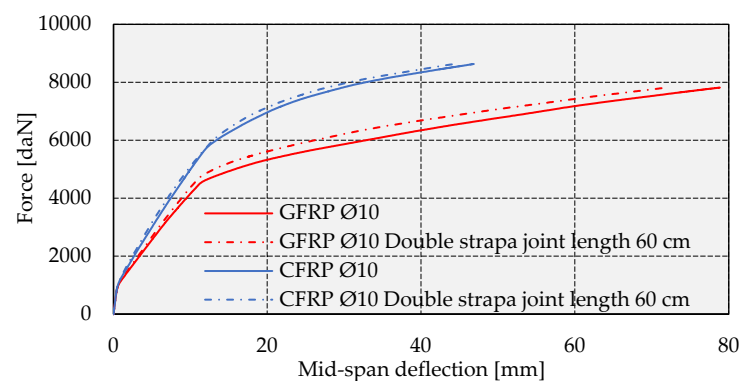


**Figure 24.** Comparative analysis of the force–deflection diagram of the CFRP and GFRP model with a double-strap joint length of 60 cm.

### 3.4. Practical and Economic Feasibility

The practical and economic aspects of the proposed double-strap joint method for FRP bar splicing have been analyzed relative to the classic lap splice method. One hypothetical RC beam with a length of 6 m, strengthened with one FRP bar of Ø10, is chosen for this analysis. Required groove sizes and the consumption of materials are compared in Table 2 for both cases of FRP splicing. The required groove cross-section for the double-strap joint method is  $20 \times 20$  mm, with the groove widening to  $50 \times 20 \times 600$  mm in the cut-off zone. In the case of the classic lap splice method, it is assumed that the groove width is equal to the double value of the required groove width for one FRP bar, i.e., the groove cross-section is  $40 \times 20$  mm, considering that such a solution provides better results regarding the beam strength compared to the solutions with two grooves (one groove for each FRP bar) [28]. It is determined that the required overlapping length is  $60\phi$  and  $110\phi$  for the double-strap joint and classic lap splice method, respectively, considering that these overlapping lengths provide beam strengths equal to cases of beams with continual additional FRP bars. It should be mentioned that this analysis covers required quantities of FRP bars, epoxy, and primer for concrete surface preparation. The consumption of epoxy is  $1.55 \text{ kg/m}^2$  per mm of thickness, and the consumption of primer is  $300 \text{ g/m}^2$ , where both values have been adopted according to the manufacturer's data [20]. Based on the conducted analysis, one may conclude that the double-strap joint method requires about 40% less groove volume/epoxy and about 25% less groove surface area/primer compared to the classic lap splice method for the analyzed case. In addition to savings in material, the required execution time is less in the case of the double-strap joint method, which is also a very important factor in such an analysis. These results should provide more benefits regardless of the negligibly higher required FRP length (less than 1.50% in the analyzed case). It is worth mentioning that a cost analysis has not been provided here, because the costs of the material and construction work are different in different countries.

**Table 2.** Economic analysis.

Splicing Method	FRP Length (m)	Groove Volume (m <sup>3</sup> )	Groove Surface Area (m <sup>2</sup> )	Epoxy (kg)	Primer (kg)
Double-strap joint	7.20 (101.41%)	0.00276 (57.50%)	0.363 (75.63%)	4.278 (57.50%)	0.109 (75.63%)
Classic lap splice	7.10 (100%)	0.00480 (100%)	0.480 (100%)	7.440 (100%)	0.144 (100%)

## 4. Conclusions

The proposed method for the splicing of the FRP bar cut-off by both-sided overlapping, called “double-strap joint NSM FRP”, showed very good results regarding providing mechanical characteristics of beams, compared to strengthening realized by a bar without a cut-off [16]. Non-linear numerical FEM models for the analysis of the behavior of beams strengthened via NSM FRP reinforcement with different overlapping splicing lengths have

been presented. The influence of the diameter and type of NSM FRP bars on the strength and stiffness of the beams has been investigated as well. In the end, the practical and economic feasibility of the double-strap joint method has been shown in comparison to the classic lap splice method. Based on the presented results, the following conclusions can be drawn:

- The results of the nonlinear numerical analysis of RC beams strengthened by the NSM FRP technique, loaded to bending according to the four-point load disposition, showed very good agreement with the experimental results regarding the load–deflection relationships, failure mechanisms, and strains in the GFRP bars. Therefore, the model is validated.
- The concrete damage plasticity material model is suitable for a numerical analysis of concrete and epoxy with the appropriate definition of the parameters of the material mechanical properties (see Sections 2.2.2 and 2.2.3).
- In most cases, beam failure occurs due to the exceeding of the shear stress between the concrete and the epoxy (bond stress) in the zone starting from the load application towards the supports as well as at the beginning of the groove for inserting the supplemental bars for splicing.
- It has been shown that an overlapping length of  $60\varnothing$  provides an increase in beam strength equal to the increase in strength in the case of an NSM FRP bar without a cut-off.
- With an increase in the diameter of the FRP bars ( $\varnothing 8$ ,  $\varnothing 10$ , and  $\varnothing 12$ ), the strength of the strengthened beams increases for about 10% in the case of GFRP bars and about 5% in the case of CFRP bars.
- Via the application of CFRP bars instead of GFRP bars, one achieves higher beam strength, but lower beam ductility, for the same diameters used. Therefore, choosing between CFRP and GFRP bars for the strengthening of the RC beam should be based on the load-bearing requirements, but with the limitation of preventing the brittle failure of the strengthened beam under the ultimate design loads.
- The failure mechanism is qualitatively the same regardless of the material of FRP bars, but in the case of CFRP a more prominent peeling-off at the concrete–epoxy joint occurs.
- Potential savings in the material and construction time are possible via the application of the proposed double-strap joint method compared to the classic lap splice method.

A numerical analysis showed that, for an overlapping length of  $60\varnothing$ , the proposed way of splicing of FRP bars with a cut-off (“double-strap joint NSM FRP”) achieves full beam strength, as in the case of FRP bars without a cut-off, regardless of the material used (GFRP or CFRP). This important conclusion is very significant for everyday engineering practices when the splicing of the additional FRP reinforcement in the NSM strengthening technique is necessary.

The scope of this paper did not encompass some other significant parameters, such as the following: surface treatment of the bars, concrete quality, groove dimensions, and groove disposition. The effectiveness of the proposed double-strap joint method has been researched for the case of pure bending, but research on other loading conditions is important as well. Defining the bypassing length of the cut-off as a function of the mentioned parameters is a task for future research in order to complete the proposed method.

**Author Contributions:** Conceptualization, S.R.; methodology, A.Z.; software, A.Z. and T.V.; validation, S.R., A.Z., T.V. and Ž.P.; investigation, S.R. and Ž.P.; writing—original draft preparation, S.R.; writing—review and editing, A.Z., T.V. and Ž.P.; visualization, S.R. and A.Z.; supervision, S.R.; project administration, S.R. All authors have read and agreed to the published version of the manuscript.

**Funding:** This research received no external funding.

**Institutional Review Board Statement:** Not applicable.

**Informed Consent Statement:** Not applicable.

**Data Availability Statement:** The data presented in this study are available on request from the corresponding author. The data are not publicly available due to privacy.

**Conflicts of Interest:** The authors declare no conflict of interest.

## References

1. ACI 440.2R-17; Guide for the Design and Construction of Externally Bonded FRP Systems for Strengthening Concrete Structures. American Concrete Institute: Farmington Hills, MI, USA, 2017.
2. Fédération internationale du béton (Fib). *Externally Applied FRP Reinforcement for Concrete Structures*; Bulletin no. 90; Fédération internationale du béton (Fib): Lausanne, Switzerland, 2019.
3. Concrete Society. *Design Guidance for Strengthening Concrete Structures Using Fibre Composite Materials*; Technical Report 55; Concrete Society: Crowthorne, UK, 2012.
4. Wattanapanich, C.; Imjai, T.; Garcia, R.; Rahim, N.L.; Abdullah, M.M.A.B.; Sandu, A.V.; Vizureanu, P.; Matasaru, P.D.; Thomas, B.S. Computer Simulations of End-Tapering Anchorages of EBR FRP-Strengthened Prestressed Concrete Slabs at Service Conditions. *Materials* **2023**, *16*, 851. [\[CrossRef\]](#)
5. El-Hacha, R.; Rizkalla, S.H. Near-Surface-Mounted Fiber-Reinforced Polymer Reinforcements for Flexural Strengthening of Concrete Structures. *ACI Struct. J.* **2004**, *101*, 717–726. [\[CrossRef\]](#)
6. De Lorenzis, L.; Teng, J.G. Near-surface mounted FRP reinforcement: An emerging technique for strengthening structures. *Compos. B Eng.* **2007**, *38*, 119–143. [\[CrossRef\]](#)
7. Al-zu'bi, H.; Abdel-Jaber, M.; Katkhuda, H. Flexural Strengthening of Reinforced Concrete Beams with Variable Compressive Strength Using Near-Surface Mounted Carbon-Fiber-Reinforced Polymer Strips [NSM-CFRP]. *Fibers* **2022**, *10*, 86. [\[CrossRef\]](#)
8. Imjai, T.; Setkit, M.; Figueiredo, F.P.; Garcia, R.; Sae-Long, W.; Limkatanyu, S. Experimental and numerical investigation on low-strength RC beams strengthened with side or bottom near surface mounted FRP rods. *Struct. Infrastruct. Eng.* **2023**, *19*, 1600–1615. [\[CrossRef\]](#)
9. Petrović, Ž.; Milošević, B.; Ranković, S.; Mladenović, B.; Zlatkov, D.; Zorić, A.; Petronijević, P. Experimental Analysis of Continuous Beams Made of Self-Compacting Concrete (Scc) Strengthened with Fiber Reinforced Polymer (Frp) Materials. *Appl. Sci.* **2021**, *11*, 4032. [\[CrossRef\]](#)
10. Asplund, S.O. Strengthening bridge slabs with grouted reinforcement. *J. Am. Concr. Inst.* **1949**, *45*, 397–406. [\[CrossRef\]](#)
11. Nanni, A. North American Design Guidelines for Concrete Reinforcement and Strengthening Using FRP: Principles, Applications, and Unsolved Issues. *Constr. Build. Mater.* **2003**, *17*, 439–446. [\[CrossRef\]](#)
12. Teng, J.G.; De Lorenzis, L.; Wang, B.; Rong, L.; Wong, T.N.; Lam, L. Debonding failures of RC beams strengthened with near-surface mounted CFRP strips. *J. Compos. Constr.* **2006**, *10*, 92–105. [\[CrossRef\]](#)
13. Bilotta, A.; Ceroni, F.; Barros, J.A.O.; Costa, I.; Palmieri, A.; Szabó, Z.K.; Nigro, E.; Matthys, S.; Balazs, G.; Pecce, M. Bond of NSM FRP-Strengthened Concrete: Round Robin Test Initiative. *J. Compos. Constr.* **2016**, *20*, 4015026. [\[CrossRef\]](#)
14. Ranković, S.; Folić, R.; Mijalković, M. Flexural behaviour of RC beams strengthened with NSM CFRP and GFRP bars—Experimental and numerical study. *Rom. J. Mater.* **2013**, *43*, 377–390.
15. Ranković, S. Eksperimentalno-Teorijska Analiza Graničnih Stanja Armiranobetonskih Linijskih Nosača Ojačanih Sprezanjem sa NSM Vlaknastim Kompozitima (Experimental and Theoretical Analysis of Limit State of Reinforced Concrete Beams Strengthened with NSM Fiber Composites). Ph.D. Thesis, University of Niš, Niš, Serbia, 2011.
16. Rankovic, S.; Folić, R.; Zorić, A.; Vacev, T.; Petrović, Ž.; Kovačević, D. Experimental Analysis of an Innovative Double Strap Joint Splicing of GFRP Bars by NSM Methods for Strengthening. *Period. Polytech. Civ. Eng.* **2023**. [\[CrossRef\]](#)
17. Anand, N.; Tattukolla, K.; Eva, L.; Mervin, E.M.; Balamurali, K.; Diana, A. Flexural Behavior of Reinforced Concrete Beams with FRP Bars Exposed to Elevated Temperature. *Period. Polytech. Civ. Eng.* **2023**, *67*, 93–101. [\[CrossRef\]](#)
18. Baena, M.; Jahani, Y.; Torres, L.; Barris, C.; Perera, R. Flexural Performance and End Debonding Prediction of NSM Carbon FRP-Strengthened Reinforced Concrete Beams under Different Service Temperatures. *Polymers* **2023**, *15*, 851. [\[CrossRef\]](#)
19. Chen, Z.; Yu, J.; Nong, Y.; Yang, Y.; Zhang, H.; Tang, Y. Beyond time: Enhancing corrosion resistance of geopolymer concrete and BFRP bars in seawater. *Compos. Struct.* **2023**, *322*, 117439. [\[CrossRef\]](#)
20. Mapei FRP System. Available online: [www.mapei.com](http://www.mapei.com) (accessed on 12 February 2023).
21. Haryanto, Y.; Hu, H.-T.; Han, A.L.; Hsiao, F.-P.; Teng, C.-J.; Hidayat, B.A.; Nugroho, L. Nonlinear 3D Model of Double Shear Lap Test for the Bond of Near-surface Mounted FRP Rods in Concrete Considering Different Embedment Depth. *Period. Polytech. Civ. Eng.* **2021**, *65*, 878–889. [\[CrossRef\]](#)
22. Berardi, V.P. Fracture Failure Modes in Fiber-Reinforced Polymer Systems Used for Strengthening Existing Structures. *Appl. Sci.* **2021**, *11*, 6344. [\[CrossRef\]](#)
23. Xia, L.; Zheng, Y. Deep Embedment (DE) FRP Shear Strengthening of Concrete Bridge Slabs under Loads Close to Supports. *Appl. Sci.* **2018**, *8*, 721. [\[CrossRef\]](#)
24. Echeverria, M.; Perera, R. Three dimensional nonlinear model of beam tests for bond of near-surface mounted FRP rods in concrete. *Compos. B Eng.* **2013**, *54*, 112–124. [\[CrossRef\]](#)
25. Gao, J.; Xu, P.; Fan, L.; Terrasi, G.P. Study on Bond-Slip Behavior between Seawater Sea-Sand Concrete and Carbon Fiber-Reinforced Polymer (CFRP) Bars with Different Surface Shapes. *Polymers* **2022**, *14*, 2689. [\[CrossRef\]](#)

26. Yu, H.; Bai, Y.L.; Dai, J.-G.; Gao, W.-Y. Finite Element Modeling for Debonding of FRP-to-Concrete Interfaces Subjected to Mixed-Mode Loading. *Polymers* **2017**, *9*, 438. [\[CrossRef\]](#)
27. Benmokrane, B.; Aly, R.; Ebead, U. Tensile Lap Splicing of Fiber-Reinforced Polymer Reinforcing Bars in Concrete. *ACI Struct. J.* **2006**, *103*, 226–234. [\[CrossRef\]](#)
28. Kadhim, M.M.A.; Jawdhari, A.; Peiris, A. Evaluation of lap-splices in NSM FRP rods for retrofitting RC members. *Structures* **2021**, *30*, 877–894. [\[CrossRef\]](#)
29. Zhou, J.; Stümpel, M.; Kang, C.; Marx, S. Lap-spliced connections of steel and FRP bars in reinforced flexure concrete structures. *Eng. Struct.* **2022**, *263*, 114409. [\[CrossRef\]](#)
30. Rolland, A.; Argoul, P.; Benzarti, K.; Quiertant, M.; Chataigner, S.; Khadour, A. Analytical and numerical modeling of the bond behavior between FRP reinforcing bars and concrete. *Constr. Build. Mater.* **2020**, *231*, 117160. [\[CrossRef\]](#)
31. D’Antino, T.; Pisani, A.P. General Analytical Model for the Bond Capacity of NSM FRP-Concrete Joints. *J. Compos. Constr.* **2020**, *24*, 04020065. [\[CrossRef\]](#)
32. Hassan, T.K.; Rizkalla, S.H. Bond Mechanism of Near-Surface-Mounted Fiber-Reinforced Polymer Bars for Flexural Strengthening of Concrete Structures. *ACI Struct. J.* **2004**, *101*, 830–839. [\[CrossRef\]](#)
33. Tepfers, R. *A Theory of Bond Applied to Overlapped Tensile Reinforcement Splices for Deformed Bars*, Publication 73:2 Division of Concrete Structures; Chalmers University of Technology: Göteborg, Sweden, 1973.
34. Tepfers, R.; De Lorenzis, L. Bond of FRP reinforcement in concrete—A challenge. *Mech. Compos. Mater.* **2003**, *39*, 315–328. [\[CrossRef\]](#)
35. *ACI 408R-03*; Bond and Development of Straight Reinforcing Bars in Tension. American Concrete Institute Committee A: Detroit, MI, USA, 2003.
36. *EN 1992:2004*; Design of Concrete Structures—Part 1-1: General Rules and Rules for Buildings. European Committee for Standardization CEN: Brussels, Belgium, 2004.
37. Wang, T.; Hsu, T.T.C. Nonlinear finite element analysis of concrete structures using new constitutive models. *Comput. Struct.* **2001**, *79*, 2781–2791. [\[CrossRef\]](#)
38. Kim, J.J.; Taha, M.R. Experimental and Numerical Evaluation of Direct Tension Test for Cylindrical Concrete Specimens. *Adv. Civ. Eng.* **2014**, *2014*, 156926. [\[CrossRef\]](#)
39. Dassault Systems. *Abaqus Theory Manual*; Dassault Systems: Providence, RI, USA, 2014.
40. Alfarah, B.; López-Almansa, F.; Oller, S. New methodology for calculating damage variables evolution in Plastic Damage Model for RC structures. *Eng. Struct.* **2017**, *132*, 70–86. [\[CrossRef\]](#)
41. Petrović, Ž.; Milošević, B.; Zorić, A.; Ranković, S.; Mladenović, B.; Zlatkov, D. Flexural Behavior of Continuous Beams Made of Self-Compacting Concrete (SCC)—Experimental and Numerical Analysis. *Appl. Sci.* **2020**, *10*, 8654. [\[CrossRef\]](#)
42. Lubliner, J.; Oliver, J.; Oller, S.; Oñate, E. A plastic-damage model for concrete. *Int. J. Solids Struct.* **1989**, *25*, 299–326. [\[CrossRef\]](#)
43. Zienkiewicz, O.; Taylor, R.L.; Zhu, J.Z. *The Finite Element Method: Basis and Fundamentals*, 6th ed.; Elsevier: Oxford, UK, 2005; pp. 398–404.
44. Seracino, R.; Raizal Saifulnaz, M.R.; Oehlers, D.J. Generic Debonding Resistance of EB and NSM Plate-to-Concrete Joints. *J. Compos. Constr.* **2007**, *11*, 62–70. [\[CrossRef\]](#)
45. Shamass, R.; Zhou, X.; Aldano, G. Finite-Element Analysis of Shear-Off Failure of Keyed Dry Joints in Precast Concrete Segmental Bridge. *J. Bridge Eng.* **2015**, *20*, 04014084. [\[CrossRef\]](#)
46. Vacev, T.; Zorić, A.; Grdić, D.; Ristić, N.; Grdić, Z.; Milić, M. Experimental and Numerical Analysis of Impact Strength of Concrete Slabs. *Period. Polytech. Civ. Eng.* **2023**, *67*, 325–335. [\[CrossRef\]](#)

**Disclaimer/Publisher’s Note:** The statements, opinions and data contained in all publications are solely those of the individual author(s) and contributor(s) and not of MDPI and/or the editor(s). MDPI and/or the editor(s) disclaim responsibility for any injury to people or property resulting from any ideas, methods, instructions or products referred to in the content.